Supporting Information

Valentine et al. 10.1073/pnas.1414873111

Hopane Data Interpolation

The hopane data used in this study represent discrete sample concentrations collected at individual core locations (*Methods*). Estimates of the total amount of hopane deposited in the study area (Fig. 5) were calculated using spatial interpolation methods based on the discrete sample concentration values. All analyses were performed using the Geostatistical Analyst Toolbox in ArcGIS 10.2 and are described below. Additional information about the individual parameters, statistics, and techniques used is available (1).

Inverse Distance Weighting. The data were explored first using inverse distance weighting (IDW), a simple interpolator that averages the values of a given number of data points in a specified search neighborhood and weights them by their distance from the interpolated point (1, 2). This technique assumes no stationarity in the data and operates under the assumption that points that are closer to one another are more similar than those farther apart. To this end, the model requires a defined maximum and minimum number of neighboring points, a search neighborhood geometry and radius, and a power function that defines the weight of the neighboring points proportional to their inverse distance. It should be noted that this method by definition preserves the exact value located at the input points where the distance is zero.

In this analysis, a constant circular search radius of 40 km was used, and variation was allowed in the maximum number of points used to interpolate at a given location. Varying the maximum number of points in the interpolation has an effect similar to varying the radius: Using a greater number of points will include points farther away, and using fewer points will, in effect, limit the search radius. An additional geometry also was tested whereby the circular geometry was split into four quadrants with the main axis oriented at a 45° angle. This geometry was chosen for two reasons: (*i*) the elevated hopane data tend to follow a 45° southwest–northeast trend, creating some overall anisotropy as it impinges on the rising topography of the continental slope, and (*ii*) the four quadrants force the interpolation to use the prescribed number of points from each quadrant, preventing spatial selectivity from a cluster of points in a limited region or direction. Last, the power-law exponent was varied using values of 1 and 3, whereby the weights of surrounding points are proportional to the inverse distance from the interpolated point raised to the prescribed exponent. In simple terms, an exponent of 0 would weight all points evenly regardless of distance, but as the exponent increases, the weights of distant points decrease rapidly. Table S1 presents the parameter setups for the IDW interpolation models.

For each IDW model cross-validation was performed. In cross-validation each input point is removed, one at a time, and the surface is interpolated again to predict the associated value using the other points. In lieu of IDW prediction errors, these cross-validation values can be compared with the input point value to obtain a general metric of the model's robustness. Ideally, the mean predicted error from the cross-validation would be close to 0, and the root mean squared error (RMSE) would be as low as possible (i.e., an RMSE and mean predicted error of 0 would be a perfect match between the predicted and the measured data points).

Results from the IDW interpolation over the study area are shown in Table S1. Mean hopane concentrations range from 170–213 $ng{\cdot}g^{-1}$ for individual runs and account for 5.8–7.5% of the total hopane discharge estimate from the Macondo Well. This calculation assumes a background hopane concentration of 28 $ng{\cdot}g^{-1}$ in the Gulf of Mexico and provides one estimate of uncertainty as to the magnitude of hopane contamination in this region. Mean predicted errors and RMSE are relatively insensitive to the range of parameters tested.

Empirical Bayesian Kriging. IDW is simplistic and fast, but kriging techniques generally require a considerable amount of decision-making and some assumptions about the stationarity and distribution of data (1, 2). Kriging statistical techniques allow a variety of output surfaces to be produced, including predictions, prediction SEs, probabilities, and quantiles, permitting better constraint and quantification of the errors associated with different parameters and interpolations. In this study, EBK was chosen as the preferred kriging method for several reasons (1, 3, 4). First, EBK automates the most difficult aspects of creating a valid kriging model by subsetting the data and running multiple semivariogram simulations to derive a best fit. This automation reduces the amount of interactive modeling and greatly simplifies the optimization of parameters. Second, EBK provides more accurate estimates of error by accounting for the uncertainty in the semivariogram, whereas other kriging methods assume that the estimated semivariogram is the true semivariogram for the entire interpolation region. Thus, other kriging methods tend to underestimate the SEs of prediction. Last, there is greater flexibility and accuracy in predictions of moderately nonstationary data using EBK than in those using other kriging methods. The primary disadvantage of EBK is that, because it is an iterative method, it can be computationally intensive with larger datasets. This drawback did not prove to be problematic in this study.

Similar to the IDW analysis, the number of maximum and minimum neighbors and the neighborhood geometry were varied. A standard circular geometry with a radius of 40 km was fixed throughout, as were the overlap factor, subset size, and number of semivariogram simulations. The overlap factor specifies the degree of overlap between subsets; at the maximum possible overlap factor of 5, each point can be used in five different simulations, creating a smoother output surface. The subset size was fixed at 20 points to improve computational efficiency and constrain the semivariogram estimate to a smaller area that better captures the inherent variability of the dataset. For each subset, a semivariogram is estimated from the data, and new data are unconditionally simulated at each of the input locations in the subset. A new semivariogram then is estimated from the simulated data and is used again to simulate new data. In this study, this process was repeated 200 times per subset, with the distribution of these simulations providing the improved statistical treatment of errors compared with other methods of interpolation. It should be noted that the overlap factor, subset sizes, and number of simulations were optimized and fixed based on computational efficiency as well as statistical fit, but the varied parameters in Table S2 were the main source of variability in error.

Results from the EBK analysis (Tables S2 and S3) demonstrate similar error statistics across parameter runs and when converted to a surface show mean hopane concentration values similar to those in the IDW analyses (Table S1), ranging from 171–209 $ng{\cdot}g^{-1}$. These concentrations represent 5.8–7.3% of the total estimated hopane released from the Macondo Well and provide a second measure of uncertainty as to the magnitude of hopane contamination in this area. The most statistically robust parameter run was EBK-C (Fig. S6 and Table S4); this

is the preferred prediction dataset used in the article (Figs. 5 and 6) as well as for statistical quantile prediction surfaces (Fig. S6 and Table S4). Ideally, a prediction surface will have a mean error close to 0, a low RMSE and average standard prediction error (these also should be close to each other in value), and a root mean squared standardized prediction error (RMSE Std) close to 1. Because EBK-C has an RMSE Std error of 0.89, it is likely that we are slightly overestimating the variability in the predictions.

Particle Deposition Modeling

Using R (version 3.0.3), we built a Monte Carlo model of particle deposition in several iterative rounds of parameter fitting. In each run, the model simulates a 2 m × 2 m patch of sediment, determining the locations of n random particles at 1-mm resolution by uniform sampling of integer points on the intervals x = [0, 2,000], y = [0, 2,000]. Particles are treated in terms of the oil masses they carried, making no assumptions about the mass or volume contribution of any nonoil material (e.g., bacterial floc). For each particle, the oil mass was sampled from a broad normal distribution, and the hopane mass fraction was sampled from a normal distribution with a mean of 58 μg hopane·g(oil)$^{-1}$ [SD, 8 μg hopane·g(oil)$^{-1}$], as calculated from the available data released by NOAA.

Next, coring is simulated by randomly choosing a 3,136-mm^2 block [the cross-section of a standard 6.35-cm (2.5-in) push-core] within the patch. The number and size of particles caught by each core then are determined, and the surficial hopane concentration signal in nanograms of hopane per gram of sample is determined as follows. First, the background sample mass is determined for a 1-cm-thick section of sediment with a dry weight of 0.38 g·cm^{-3} (*Methods*). Second, for any particles caught by the core, the simulated oil mass and hopane mass fraction are used to calculate the particle-borne hopane mass. Third, the core is assigned a background hopane signal, drawn at random from the distribution of measured background-level (<75 ng·g^{-1}) surficial hopane concentrations in the dataset. Finally, the hopane concentration is calculated as the sum of background (adjusted to account for the additional oil mass) and signal (excess hopane mass divided by the sum of dry sediment mass and excess oil mass) concentrations. Note that this calculation is derived from the hopane concentration and does not include the mass of any nonoil components of the particle.

The resulting distribution of simulated surficial hopane concentrations was compared with the distribution measured in 707 cores at 534 sampling sites. In initial fitting, the model permitted a single mean oil mass; repeated rounds of simulation (10^3 runs per set of parameters) were used to scan an average of 5 ng–5 g oil per particle and 10–10^6 particles per 2 m × 2 m patch (Fig. S2). At particle densities >10^4 per patch, cores are very likely to capture at least one particle, leaving too few background-level cores; at lower spatial densities, an oil mass ≤0.25 mg is insufficient to shift the surficial hopane concentration substantially, whereas an oil mass of ∼5 g per particle causes too great a shift, with no way to populate the substantial peak at 100–200 ng·g^{-1}. We therefore focused on spatial densities of 10–1,000 particles per patch and oil masses of 3.4 mg–1.8 g. In addition, because no single mean oil mass could regenerate the multimodal form of the observed distribution of surficial hopane concentrations, we moved to a mixed model of relatively common oil-poor particles, less common midrange particles, and rare oil-rich particles. In four successive rounds of χ^2 minimization, we alternated between refining the number and the mean oil mass of each type of particle. The final fitted values (800 particles with a mean oil mass of 0.024 g per 2 m × 2 m patch, 90 particles with a mean oil mass of 0.19 g, and 20 particles with a mean oil mass of 1.13 g) gave χ^2 = 1,934 with 706 degrees of freedom (Fig. S3).

To assess the heterogeneity of surficial hopane concentration signals expected from this model, we simulated sampling two, three, four, or five disjoint cores from each of 10,000 patches (2 m × 2 m) generated using the optimized parameters. As before, we calculated the surficial hopane concentration for each core; in addition, we then calculated the mean and SD of each single-site set of simulated hopane concentrations, obtaining a set of 10,000 paired single-site mean and SD values for two-core simulations, a second set for three-core simulations, a third for four-core simulations, and a fourth for five-core simulations. These values are plotted as black points in Fig. 3; as expected, the distribution becomes more compact as the number of cores per site increases. Finally, we calculated the mean and SD of surficial hopane concentration measurements at each of the 117 sampling sites at which multiple parallel cores were collected and compared these observations (red points in Fig. 3) with the simulation.

Background Hopane Concentration

To define hopane contamination from the *Deepwater Horizon* event, an estimate of background hopane concentration was needed. A search of published literature and government reports failed to provide prespill hopane concentrations for surficial sediments in the northeast Gulf of Mexico. Therefore, on the assumption that surficial hopane concentrations measured close to the well are more likely to reflect contamination, and distant measurements are more likely to reflect the regional background, the regional distribution of surficial hopane was analyzed with respect to distance from the Macondo Well. This analysis shows that mean surficial hopane concentration decreases as distance increases to 40 km but remains roughly constant at 28 ± 23 ng·g^{-1} at greater distances (n = 70), suggesting that 28 ng·g^{-1} represents the regional mean background concentration of hopane in surficial sediments (Fig. S4). This approach likely provides an upper estimate of the background concentration, because some of the samples collected at distances >40 km may have been contaminated with low concentrations of Macondo oil. The mean background estimate of 28 ng·g^{-1} shows little sensitivity to the distance threshold chosen so long as the distance is greater than 40 km (Fig. S4).

The calculated mean background concentration was consistent with several patterns observed within 40 km of the Macondo Well. (*i*) Hopane's sediment depth distribution revealed that sediment collected beneath the surface layer typically was within the range observed for surficial samples collected >40 km from the well (e.g., Fig. 2). (*ii*) Surficial hopane concentrations within the background range are present within 40 km of the Macondo Well, as is consistent with some proximal areas receiving lesser inputs of oil. (*iii*) Clusters of samples within the 40-km radius are within the background range; notably, for samples collected at a water depth >1,700 m the mean surficial hopane concentration (±SD) was 51.7 (±34.5) ng·g^{-1} (n = 47). Although not conclusive, these observations are broadly consistent with our estimate of 28 ng·g^{-1} as a reasonable choice of mean background concentration.

To calculate the excess hopane in the vicinity of the Macondo Well, the mean background concentration (28 ng·g^{-1}) was subtracted from the total calculated mean concentration in the contaminated region (170–213 ng·g^{-1}; see *Inverse distance weighting*, above). The mean concentration of surficial hopane within 40 km of the Macondo Well is substantially higher than the background value of 28 ng·g^{-1}, and thus the calculation of excess hopane is relatively insensitive to small changes in the background concentration.

In addition to the mean background surficial hopane concentration, we sought to establish a cutoff value that could be used to determine with high confidence whether a given sample is marked by contamination with Macondo oil. The surficial hopane concentration is <75 ng·g^{-1} in >95% of samples

collected outside the 40-km contamination radius (Fig. S4); therefore we used 75 ng·g^{-1} as a threshold value and considered higher measurements as showing evidence of likely contamination. Some patterns in the data emerge at higher threshold concentrations (e.g., 100 ng·g^{-1} in Fig. 2*B*), presumably because the signal from Macondo oil begins to dominate background variability.

Accessing NRDA Data

The data used in this study were downloaded from www.gulfspillrestoration.noaa.gov/oil-spill/gulf-spill-data/ on January 1, 2014. The data were identified by the category of sediment and were located under the radio button titled "NRDA data by category."

Limitations of This Study

In this study, we argue that the observed hopane anomaly is caused by discharged Macondo oil; that the observed anomaly implies deposition of ∼12% (range 4–31%) of the oil trapped in deep intrusion layers to the sea floor; and that the observed anomaly is best explained by the deposition of a heterogeneous range of oil-bearing particles from the intrusion layers. Each of these arguments carries caveats. First, no hydrocarbon has been shown to be unique to Macondo oil, to permit definitive identification of discharged Macondo oil. Instead, our identification is based on the spatial distribution of the hopane anomaly, which is best explained by a point source at the Macondo Well. In the absence of any reasonable alternative, we consider this interpretation to be robust and advance this argument with a high degree of certainty. Second, our estimates of the extent of hopane contamination in the study area entail the propagation of multiple uncertainties and could be biased toward the low side by the necessary exclusion of several potential hopane reservoirs (as discussed in the main text). We therefore view these calculations with a moderate degree of certainty and consider our final estimate to be a likely lower bound. Third, although available information is consistent with our proposed mechanism for the deposition of oil from the deep intrusion layers to the sea floor, the data are insufficient to make a robust conclusion. We present this mechanism with a low degree of certainty.

The determination of error in the scaling calculation propagates uncertainties in several parameters (as described in the main text), including the hopane concentration in Macondo oil, sediment porosity, total oil discharge to the deep ocean, and the background hopane concentration. We include no explicit estimate of error for the assumed volume of the contaminated area or the assumed sediment density; furthermore, we were unable to assess analytical error for individual hopane measurements used to calculate the average contamination level, typically on the order of 10–20%. In addition to our preferred EBK estimate (and the associated error based on these assumptions), we suggest that the estimate should be bounded at the low end by the lowest EBK estimate minus one SD and at the high end by the highest EBK estimate plus one SD (Table S3).

1. ArcGIS Online Help 10.2. Environmental Systems Research Institute, Inc. (ESRI). http://resources.arcgis.com/en/help/main/10.2/). Accessed February 10, 2014.
2. Webster R, Oliver MA (2007) *Geostatistics for Environmental Scientists* (John Wiley & Sons, Ltd., West Sussex).
3. Chilès J-P, Delfiner P (1999) *Geostatistics: Modeling Spatial Uncertainty* (John Wiley & Sons, Inc., New York).
4. Pilz J, Spöck G (2008) Why do we need and how should we implement Bayesian kriging methods. *Stochastic Environ Res Risk Assess* 22(5):621–632.

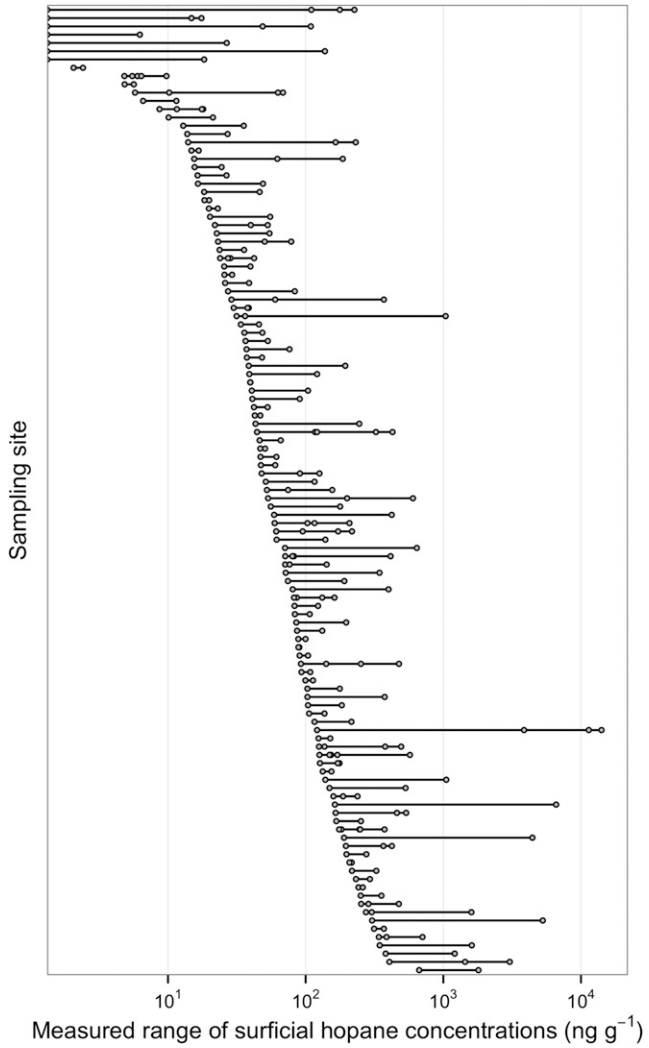

Fig. S1. Meter-scale lateral variability in surficial hopane concentrations measured in multiple parallel cores. Sets of two, three, four, or five cores were collected in parallel at 117 sampling sites; sites are ordered on the *y* axis by minimum reported surficial hopane concentration, and all measurements for a given site's cores are shown as gray points. Note that the *x* axis is on a log scale.

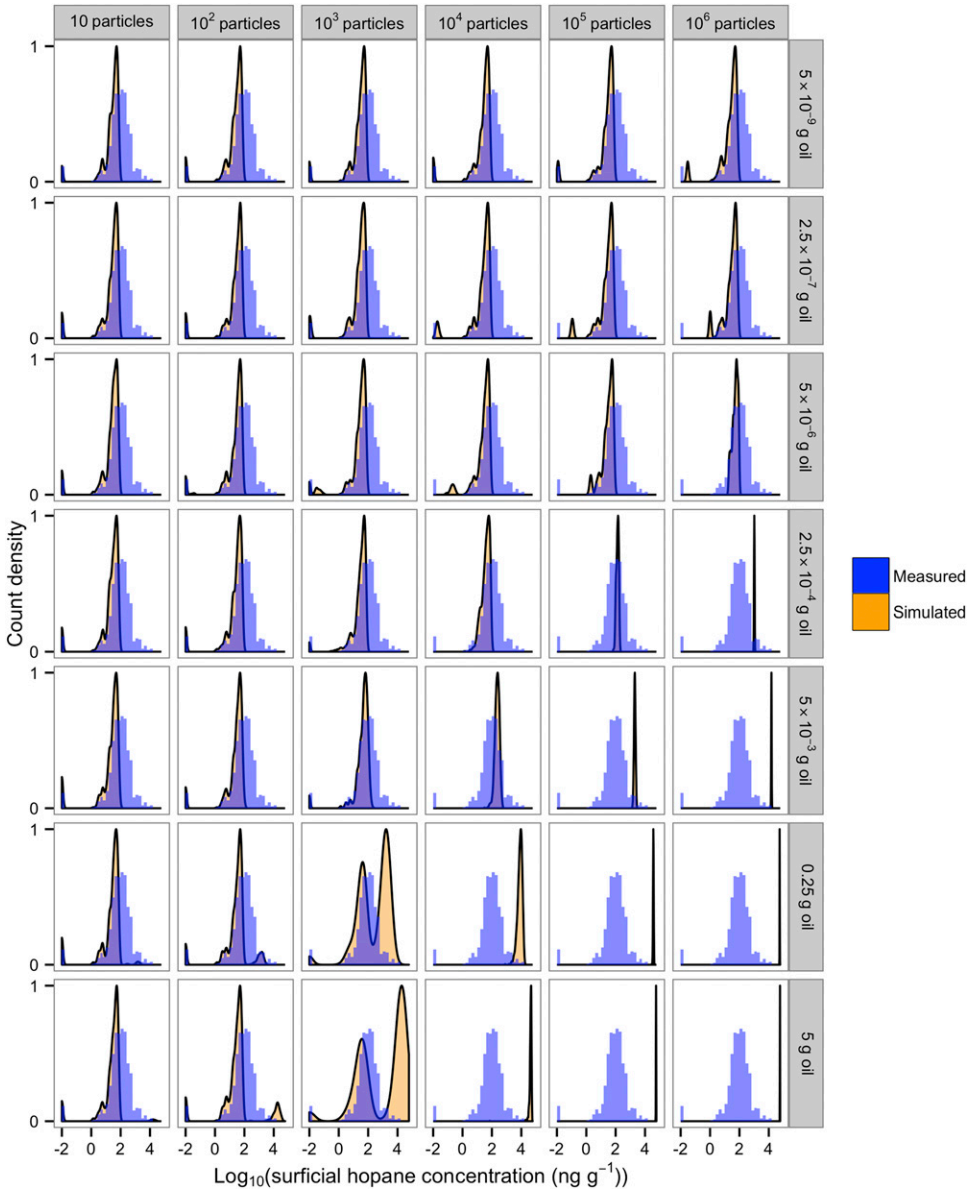

Fig. S2. Results of the initial round of particle deposition model fitting, demonstrating that the distribution of measured surficial hopane concentrations is not well fitted by a model in which particle spatial density is high or in which particle sizes cluster around a single value. Model refinement proceeded to investigate a combination of particles bearing small (~0.02 g), medium (~0.2 g), and large (~1 g) oil masses at decreasing probabilities.

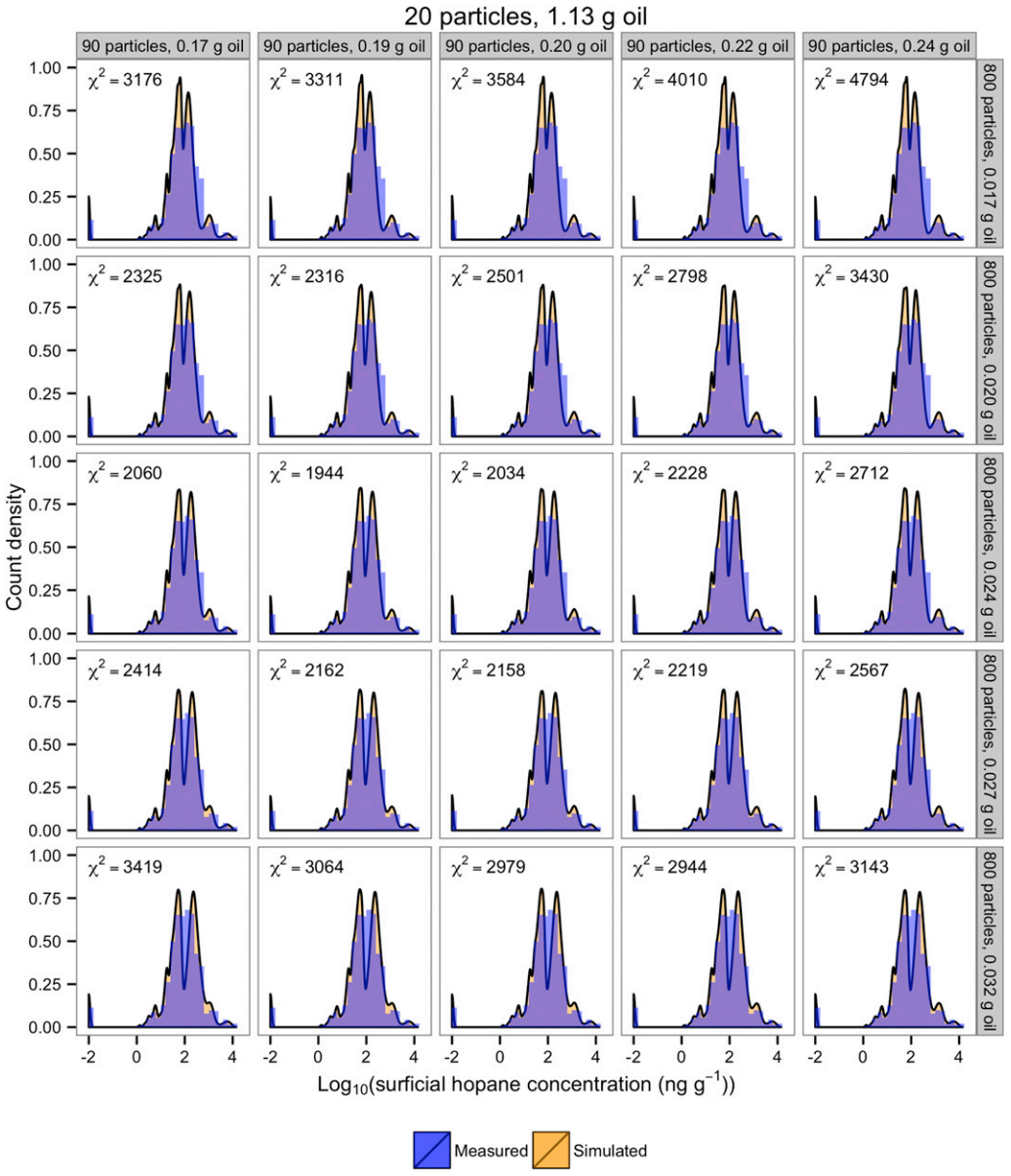

Fig. S3. Results of the final round of particle deposition model fitting, showing only the results for the optimal value of 1.13 g oil per oil-rich particle. χ^2 minimization identified the successful model as containing 800 oil-poor (mean oil mass, 0.024 g), 90 medium (mean oil mass, 0.19 g), and 20 oil-rich (mean oil mass, 1.13 g) particles per 2 m × 2 m patch of sediment.

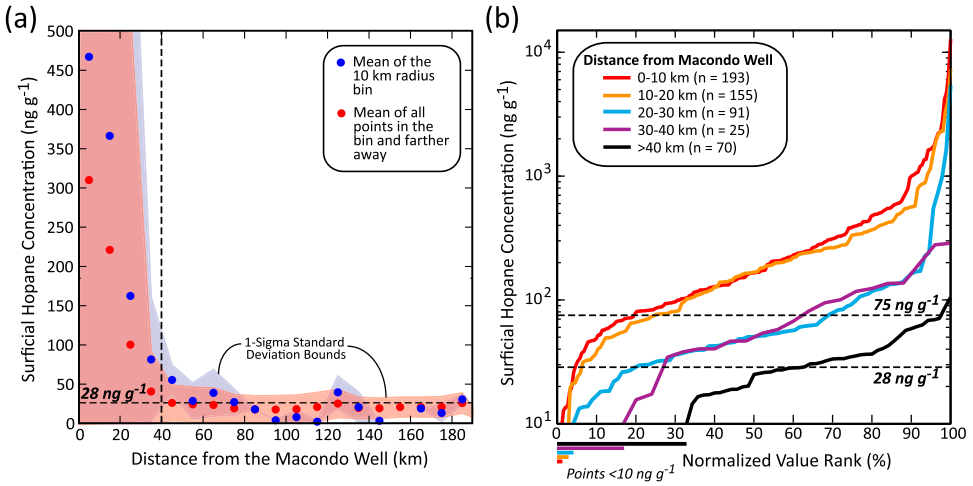

Fig. S4. Relationships between surficial hopane concentration and distance from the Macondo Well highlighting the empirically derived background value of 28 ng·g^{-1}. (*A*) Mean hopane concentrations calculated in 10-km radial bins (blue dots) from the Macondo Well along with the evolving mean concentration (red dots), which is calculated using the data from the given bin along with data from all more distal bins. Red and blue envelopes correspond to the respective colored points and indicate ±1 SD about the means. The background hopane value of 28 ng·g^{-1} is derived from the mean of the data >40 km distant from the Macondo Well as indicated by the vertical line. (*B*) Normalized rank plot for five individual bins showing decreasing hopane values with increasing distance from the source. Note that the background hopane concentration of 28 ng·g^{-1} is greater than ∼60% of the points found in the >40-km distance bin.

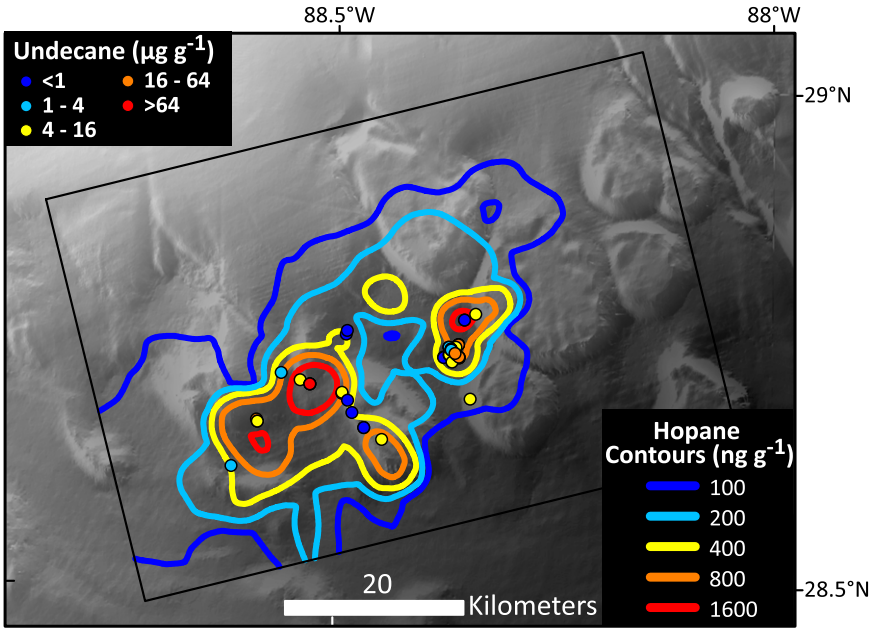

Fig. S5. Concentration of undecane (n = 51) overlaid on the interpolated hopane contours and study area as in Fig. 6*B* in the main text.

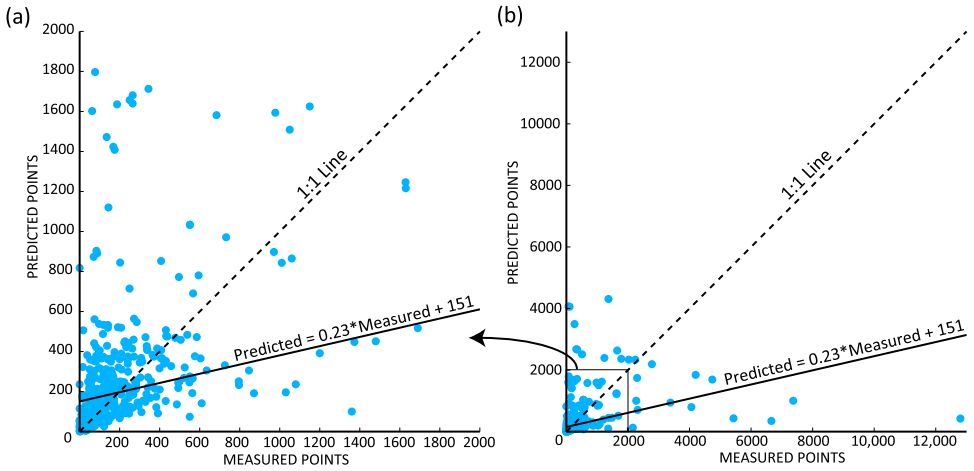

Fig. S6. EBK-C cross-validation plot zoomed in (*A*) and with all data (*B*), showing the line of best fit. Fit statistics are provided in Table S5.

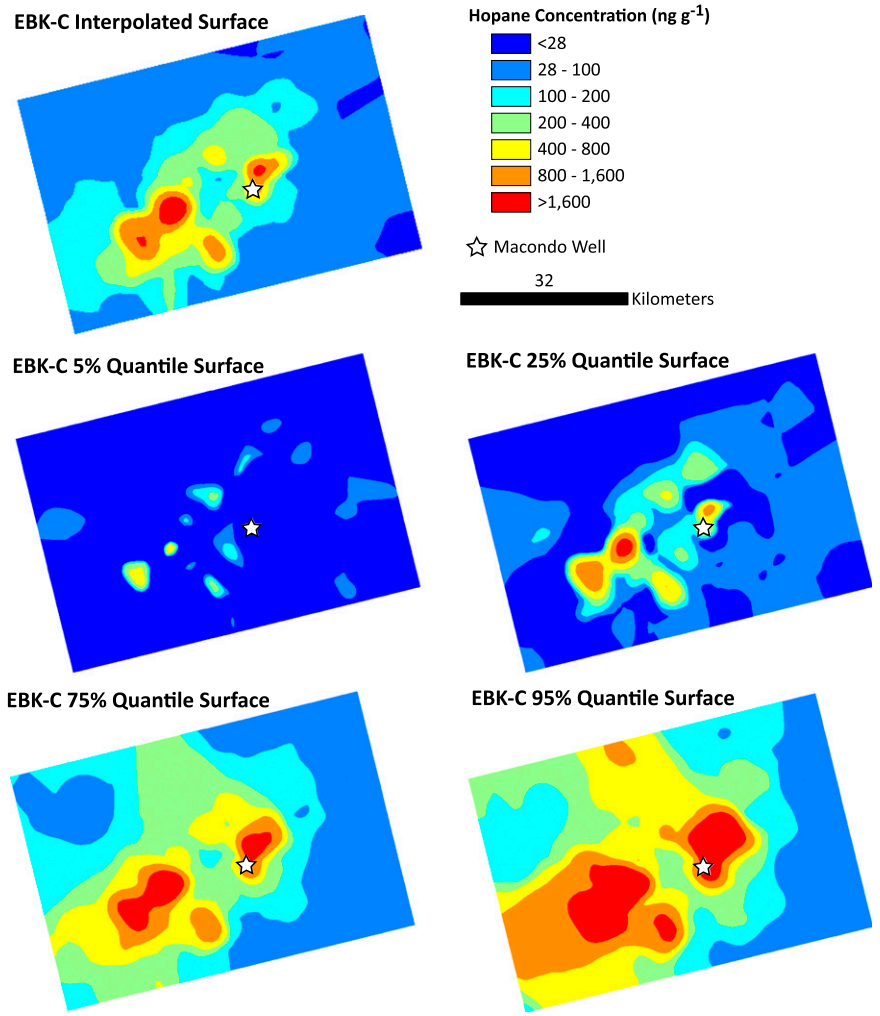

Fig. S7. EBK-C interpolated prediction surface and quantile prediction surfaces smoothed using a 2-km circular smoothing kernel for enhanced viewing. Statistics are provided in Table S4.

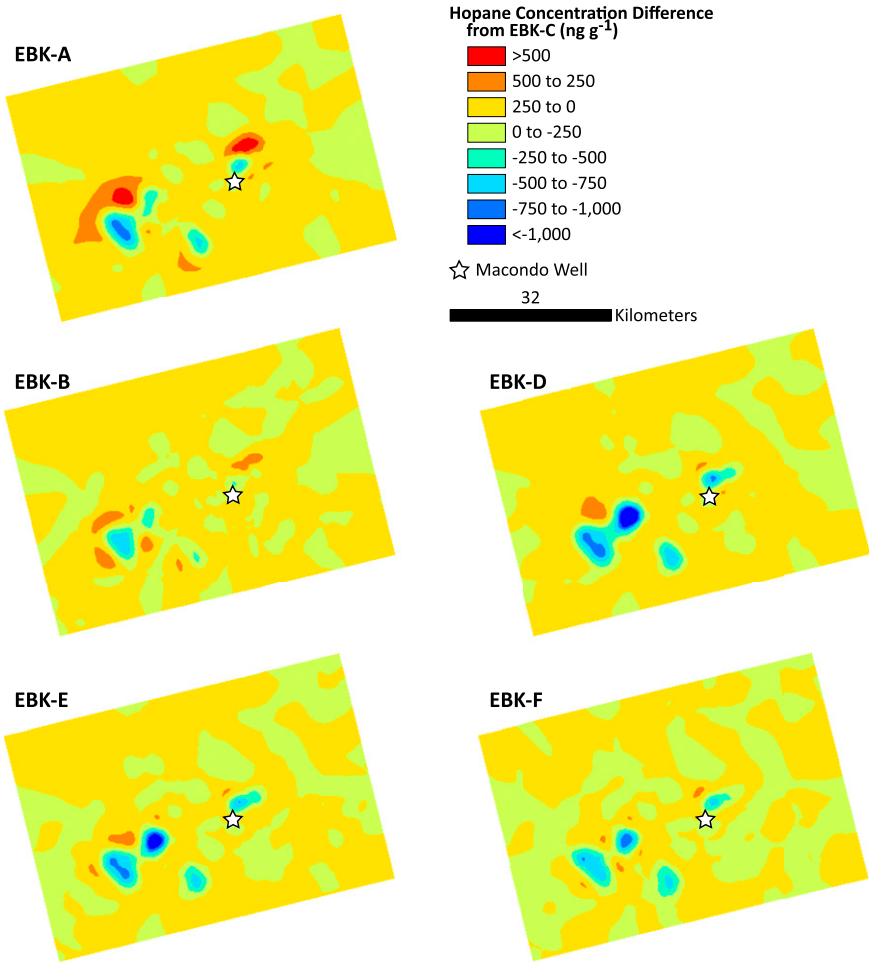

Fig. S8. Interpolated surface concentration differences between EBK-C and EBK-A through EBK-F smoothed using a 2-km circular smoothing kernel for enhanced viewing. Positive values indicate higher concentrations than EBK-C, and negative values indicate lower concentration values than EBK-C.

Table S1. IDW interpolation surface parameters and results using a 40-km radius standard circular search neighborhood

ID	Power	Maximum no. of neighbors	Minimum no. of neighbors	Sector type	RMSE	Mean error*	Mean hopane, $ng \cdot g^{-1}$†	% total hopane‡
IDW-A	1	20	10	1 sector	996	33.1	213	7.5
IDW-B	3	20	10	1 sector	1,059	20.8	184	6.3
IDW-C	1	5	3	1 sector	1,022	18.4	174	5.9
IDW-D	3	5	3	1 sector	1,058	14.6	170	5.8
IDW-E	1	10	5	4 sectors at 45°	976	24.6	203	7.1
IDW-F	3	10	5	4 sectors at 45°	1,058	20.8	184	6.3
IDW-G	1	5	3	4 sectors at 45°	990	20.3	181	6.2
IDW-H	3	5	3	4 sectors at 45°	1,057	17.6	175	6.0

*Mean prediction error from cross validation.

†Mean hopane concentration inside the defined study area (Fig. 5).

‡Percent of the total estimated hopane discharged from the Macondo Well calculated using the mean hopane value minus the estimated background value of 28 $ng \cdot g^{-1}$.

Table S2. EBK interpolation surface parameters and cross-validation statistics using a 40-km radius standard circular search neighborhood, an overlap factor of 5, and a subset size of 20 points with 200 semivariogram simulations per subset

ID	Maximum no. of neighbors	Minimum no. of neighbors	Sector type	Mean*	Mean Std†	RMSE	RMSE Std	Average SE‡
EBK-A	20	10	1 sector	12.1	0.03	817	0.77	932
EBK-B	10	5	1 sector	14.2	0.03	811	0.83	923
EBK-C	5	3	1 sector	4.1	0.02	881	0.89	954
EBK-D	10	5	4 sectors at 45°	5.3	0.02	812	0.69	932
EBK-E	5	3	4 sectors at 45°	−4.0	0.02	803	0.71	914
EBK-F	3	2	4 sectors at 45° −8.1	−8.1	0.02	827	0.76	904

*Mean prediction error.
†Mean standardized prediction error.
‡Average standard prediction error.

Table S3. EBK hopane concentration interpolation results from the study area

ID	Mean, ng·g^{-1}*	Maximum, ng·g^{-1}	Minimum, ng·g^{-1}	SD, ng·g^{-1}	% total hopane†
EBK-A	209	5,976	20	321	7.3
EBK-B	192	6,118	16	337	6.6
EBK-C	179	6,020	15	370	6.1
EBK-D	184	2,945	19	218	6.3
EBK-E	175	3,477	7	249	6.0
EBK-F	171	4,228	16	281	5.8

*Mean hopane concentration inside the defined study area (Fig. 5).
†Percent of the total estimated hopane discharged from the Macondo Well calculated using the mean hopane value minus the background value of 28 ng·g^{-1}.

Table S4. Sample points (n = 461) and EBK-C hopane concentration interpolation quantile results from the study area

Quantile	Mean, ng·g^{-1}*	Maximum, ng·g^{-1}	Minimum, ng·g^{-1}	SD, ng·g^{-1}	% total hopane†
Points	355	12,800	0	931	13.2
5%	<0	3,632	<0	428	0.0
25%	53	5,270	<0	278	1.0
Mean	179	6,020	15	370	6.1
75%	306	7,336	17	514	11.3
95%	587	9,060	33	841	22.6

*Mean hopane concentration inside the defined study area (Fig. 5).
†Percent of the total estimated hopane discharged from the Macondo Well calculated using the mean hopane value minus the background value of 28 ng·g^{-1}.

Table S5. Estimates of pure oil droplet aggregation necessary to produce particles bearing the oil masses fitted in the particle deposition model

Oil mass, g	No. of droplets with a 25-μm radius	No. of droplets with a 50-μm radius
0.02	4.4×10^5	5.5×10^4
0.19	3.5×10^6	4.4×10^5
1.1	1.9×10^7	2.4×10^6

Other Supporting Information Files

Dataset S1 (XLS)